J Nanopart Res (2012) 14:1233
DOI 10.1007/s11051-012-1233-6

RESEARCH PAPER

Advanced functionalization of organoclay nanoparticles by silylation and their polystyrene nanocomposites obtained by miniemulsion polymerization

R. Ianchis · M. C. Corobea · D. Donescu · I. D. Rosca · L. O. Cinteza · L. C. Nistor · E. Vasile · A. Marin · S. Preda

Received: 22 March 2012 / Accepted: 5 October 2012 / Published online: 21 October 2012

Abstract Four types of alkoxysilanes with different organosilyl groups were used for the silylation of a commercial alkylammonium-modified montmorillonite (Cloisite 30B). TGA, XPS, DLS, FTIR, XRD, and contact angle measurements were performed for the characterization of the silylated clays. Furthermore, the behavior of these advanced hydrophobic clays in the miniemulsion polymerization process of styrene and the characterization of nanocomposites materials were followed. The hydrophobic nature is a combined result of the length of the organic chain and of the amount of silane groups grafted onto clay edges, reflected also in the final properties of the nanocomposite latexes.

Keywords Hydrophobic clay · Nanoparticles functionalization · Miniemulsion polymerization · Polystyrene · Nanocomposites

Introduction

Recently, a wide variety of novel functional nanomaterials were synthesized by miniemulsion polymerization. During the miniemulsion polymerization, nanoparticles made of organic or inorganic materials can be encapsulated into polymers resulting in new materials with numerous applications (Landfester and Weiss 2010; Mittal 2010. The fact that the costabilizer hinders the monomer diffusion makes possible to control the morphology of the nanocomposite particles (Schork et al. 2005; Hu et al. 2010). Polymer–clay nanocomposites were prepared via miniemulsion polymerization of styrene, butylacrylate, methylametacrylate, or their mixtures. The first report on encapsulation of Laponite platelets in polystyrene via miniemulsion polymerization was published by Sun et al. (2004). Moraes et al. (2006)

R. Ianchis · M. C. Corobea (✉) · D. Donescu
National Research & Development Institute for Chemistry and Petrochemistry, ICECHIM, Spl. Independentei nr. 202, 6th District, Bucharest, Romania
e-mail: mcorobea@yahoo.com

I. D. Rosca
Department of Mechanical and Industrial Engineering, Concordia Center for Composites, Concordia University, 1515 Ste. Catherine West 4-145, Montreal, QC, Canada

L. O. Cinteza
Faculty of Chemistry, University of Bucharest, M. Kogalniceanu, 5th District, 70709 Bucharest, Romania

L. C. Nistor
"Petru Poni" Institute of Macromolecular Chemistry, 41A Grigore Ghica Voda Alley, 700487 Iasi, Romania

E. Vasile
Research & Development METAV, CA Rosetti 31, 2nd district, Bucharest, Romania

A. Marin · S. Preda
Institute of Physical Chemistry "Ilie Murgulescu", Romanian Academy, Spl. Independentei 202, 6th district, P.O. Box 194, 0600021 Bucharest, Romania

obtained cetyltrimethyl ammonium chloride-modified clay-poly(styrene-*co*-butyl acrylate). Tong and Deng (2006) synthesized polystyrene-encapsulated nanoclay composite latex via miniemulsion polymerization. Mirzataheri et al. (2009) report nanocomposite particles with core–shell morphology obtained by miniemulsion copolymerization of styrene and butyl acrylate in the presence of commercial clay. Faucheu et al. (2010) in their review article investigate the synthesis of structured clay/polymer nanocomposites by miniemulsion polymerization. They observed two types of particle morphology, clay nanoparticles either covering the surface or embedded inside the polymer particle.

Successful exfoliation of hydrophilic clays into hydrophobic polymer matrices is paramount for improving mechanical properties and to control gas permeation (Bitinis et al. 2011; Lungu et al. 2012). To increase the compatibility between the clay and the polymer matrix, the clay is rendered hydrophobic either by ion exchange with ammonium or phosphonium compounds of organic cations or by edge covalent bonding using silylating agents. Paiva et al. (2008) investigated the reaction between different types of clay and silane. Voorn et al. (2006) functionalized clay with monoalkoxy methacryloxy derivates then they encapsulated the modified montmorillonite in polymethylmethacrylate by surfactant-free starved-feed emulsion polymerization. Negrete Herrera et al. functionalized Laponite clay at platelets edges with *g*-methacryloxy propyl trimethoxysilane. The modified Laponite nanoparticles were then used in emulsion copolymerization of styrene and butyl acrylate (Herrera et al. 2004). Polyethylene nanocomposites based on trimethylchlorosilane-functionalized clay were produced by melt blending (Zhang et al. 2006). Sodium montmorillonite clay and quaternary ammonium tallow ions intercalated clay were modified with 3-aminopropyltriethoxysilane and then melt-compounded with polybutylene terephthalate (Wan et al. 2008).

Recent studies (Ianchis et al. 2011; Donescu et al. 2011; Piscitelli et al. 2010) evidenced that the organosilyl groups have a strong influence on the physical and chemical properties of the nanocomposite. Silylated MMT was successfully encapsulated inside snow-man like particles of polystyrene by surfactant-free emulsion polymerization (Ianchis et al. 2009). De Maria et al. recently reported the silylation of sodium montmorillonite and alkyl ammonium-modified montmorillonite using chlorodimethyl-octadecylsilane. The functionalized montmorillonites were used in intercalative polymerization of methylmethacrylate (De Maria et al. 2011).

Our goal is to synthesize highly hydrophobic montmorillonites and to assess their behavior in modified clay/polystyrene nanocomposites obtained via miniemulsion polymerization of styrene.

Experimental

Materials

Commercial organoclay (Closite 30B) modified with bis(2-hydroxyethyl) methylhydrogenated tallow ammonium salt was purchased from Southern Clay Products Inc.

Dichloromethane from Chimreactiv and the alkoxysilanes (trimethyl ethoxysilane, vinyl dimethylethoxysilane, phenyl dimethylethoxysilane, octyl dimethylmethoxysilane, and octadecyl dimethylmethoxysilane) from Aldrich and were used without further treatment.

Styrene (Acros Organics) was purified by distillation under reduced pressure before use. The surfactants, sodiumdodecylsulphate and Brij96V (Fluka), ammonium persulphate (APS) from Loba Feinchemie, and *n*-hexadecane from MERCK-Schuchardt were used as supplied.

Method

Silylation of clay

Figure 1 presents schematically edge-functionalized Cl30B clay with the following silanic groups: vinyl (Cl30BVy), phenyl (Cl30BPh), octyl (Cl30BC8), and octadecyl (Cl30BC18). Silylating agents were monoalkoxysilanes with different organic groups: vinyl dimethylethoxysilane (VyMe2ES), phenyl dimethylethoxysilane (PhMe2ES), octyl dimethylmethoxysilane (C8Me2MS), and octadecyl dimethylmethoxysilane (C18Me2MS).

For a typical silylation reaction, 4 g of dried Cl30B and 250 mL CH_2Cl_2 were introduced in a three-necked round bottom flask. The mixture was sonicated using a tip sonicator for 10 min on an ice bath. The flask was then equipped with a mechanical stirrer and a

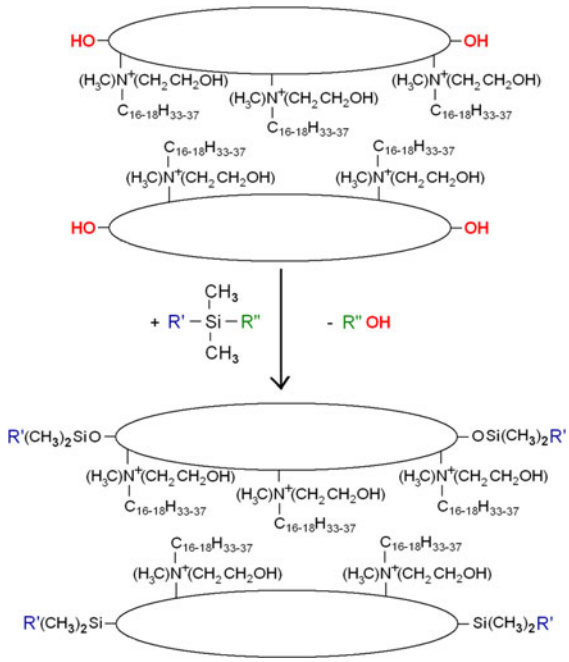

Fig. 1 Silylation schematics of organo-modified montmorillonite (Cl30B); R′—vinyl, phenyl, octyl, octadecyl and R″—methoxy, ethoxy

condenser. The mixture was stirred at 300 rpm and kept under purified nitrogen gas for 30 min. The alkoxysilanes were added drop wise. Then the reaction mixture was heated to 40 °C and refluxed for 24 h. The reaction product was centrifuged and washed with 300 mL CH_2Cl_2. After drying in a vacuum oven at 60 °C for 12 h, the final product was ground to powder.

Miniemulsion polymerization

A mixture of 0.3 g Brij 96V, 0.49 g *n*-hexadecane, 9.99 g styrene, and 0.5 g Cl30B or modified Cloisite (5.005 % wt to monomer) was sonicated for 5 min, then vigorously stirred (500 rpm) for 30 min under nitrogen atmosphere. The mixture was sonicated again for 5 min on an ice bath. Next, a solution of 0.3 g SDS in 40 g of distilled water (DW) was added to the mixture and the temperature was raised to 70 °C. The polymerization was initiated by adding 0.15 g of APS solution in 10 g of DW water. After 5 h of polymerization, the latex was cooled to room temperature. Monomer conversions were determined by the gravimetric method. Samples for analysis were prepared by casting small amounts of latex on polyethylene foil and the water was allowed to evaporate at room temperature for several days.

Analysis

Fourier transform infrared (FTIR) spectra were registered on a Brucker TENSOR 37 instrument using KBr pellets at 40 scans with 4 cm^{-1} resolution in the 4,000–400 cm^{-1} spectral range (0.3125 wt% sample in KBr).

TGA analyses were performed with a TA Q50 Instrument. The samples were heated, in dry nitrogen atmosphere with a rate of 20 °C/min. Differential scanning calorimetry (DSC) thermographs were recorded with a DSC Q200 instrument at a heating rate of 10 °C/min under nitrogen atmosphere.

The surface energy of the organo-modified clays was calculated from contact angle values. The measurements of contact angles of various liquids were performed on clay disks prepared from Cloisite powders compacted using a hydraulic press (30 MPa) at room temperature. 15-mm-diameter and 3- to 4-mm-thick samples were stored in a desiccator. The contact angle measurements were performed with a DataPhysics instrument OCA 20 and computation of surface energy from the contact angle was performed using the instruments' software. The value of the contact angle was the average value of five measurements. Glycerol and 1-bromonaphthalene were used as reference liquids. The surface energy of the solid material, and its dispersive and polar components were determined using the Owens, Wendt, Rabel, and Kaelble model (OWRK) (Owens and Wendt 1969).

XRD analyses were performed using a RIGAKU Ultima IV Instrument with Parallel Beam geometry and Ultima IV In-plane Goniometer at 40 kV/30 mA (Cu Kα), in 2θ range: 1°–30° and 5° scanning speed.

Diluted latex samples casted on aluminum stubs and copper grids were investigated by scanning electron microscopy (SEM-FEI Quanta 200) and transmission electron microscope (TEM-TECNAI F30 G^2), respectively.

Dynamic light scattering (DLS) and Laser Doppler Velocimetry (LDV) was used to determine the particles size distribution and the zeta potential, respectively (Zetasizer Nano ZS instrument Malvern Instruments Ltd.).

Surface analysis performed by X-ray photoelectron spectroscopy (XPS) was carried out on Quantera SXM equipment at 10^{-9} Torr of vacuum. The X-ray source used Al K_α radiation (1486.6 eV, monochromatized)

and the overall energy resolution was estimated at 0.65 eV by the full width at half maximum (FWHM) of the Au4f$_{7/2}$ line. To compensate the charging effect, the binding energies (BEs) were calibrated against the C1s line (BE = 284.8 eV, C–C (CH)$_n$ bonding) of the adsorbed hydrocarbon. The calculations were performed assuming that the samples were homogeneous within the detected volume. The errors in our quantitative analysis (relative concentrations) were in the range of ±10 %, while the accuracy for BEs assignments was ±0.2 eV.

Results and discussion

Characterization of functionalized clay

As expected, FTIR spectra of all samples revealed the montmorillonite specific peaks: around 1,047 cm^{-1} attributed to Si–O–Si stretching vibration and between 400 and 600 cm^{-1} attributed to Si–O bending and stretching vibration, respectively (Fig. 2). The intensity ratio of the alkyl (2,957 cm^{-1}) and that of surface hydroxyl groups (3,633 cm^{-1}) (AlAlOH, AlMgOH, and isolated SiOH) were used to prove the clay functionalization (Xu et al. 2009; Zhang et al. 2006). From Table 1, it is clear that the amount of alkyl groups is increasing with the length of hydrocarbon chain from vinyl to octadecyl. At a first look, C18 alkoxysilane seems the best candidate for Cl30B grafting.

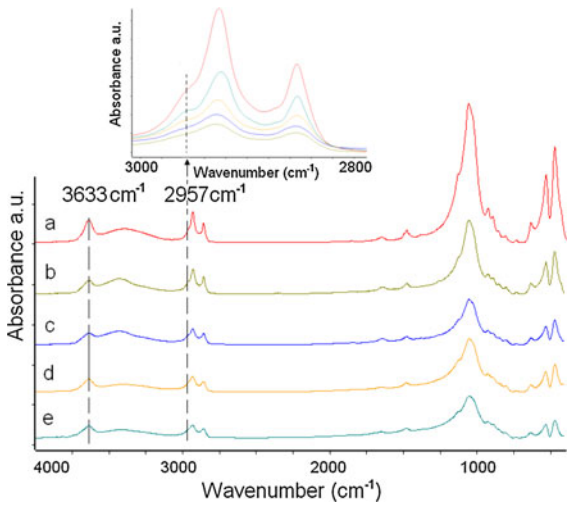

Fig. 2 FTIR spectra of Cl30B modified with monoalkoxysilanes [(*a*) Cl30B, (*b*) Cl30B-Vy, (*c*) Cl30B-Ph, (*d*) Cl30B-C8, (*e*) Cl30B-C18]

Table 1 FTIR intensity ratio calculated for Cl30B and silylated Cl30B

Cloisite type	I_1 (3,633 cm^{-1})	I_2 (2,957 cm^{-1})	I_2/I_1
Cl30B	0.281	0.165	0.587
Cl30B-Vy	0.058	0.040	0.689
Cl30B-Ph	0.110	0.082	0.745
Cl30B-C8	0.057	0.046	0.807
Cl30B-C18	0.066	0.063	0.954

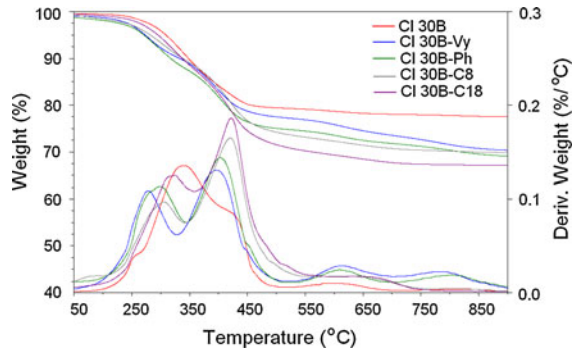

Fig. 3 Thermogravimetric and DTG plots for Cl30B and silane-modified Cl30B

Figure 3 presents TGA and DTG curves of both Cl30B as received and the silylated Cl30B, respectively. Cl30B displays mainly two decomposition intervals one in the range of 200–500 °C that corresponds to the olefin and amine decomposition (Qian et al. 2009) with a maximum peak at about 340 °C with a shoulder at about 420 °C. The other interval, between 500 and 900 °C, can be attributed to the loss of structural hydroxyl water (Wan et al. 2008; Voorn et al. 2006; Zhang et al. 2006). For the silylated derivatives, DTG curves display a new peak at 430 °C attributable to the decomposition of silane moieties. Regarding the first interval 200–500 °C, it can be observed a maximum peak at around 440 °C with a shoulder at around 270 °C. The peaks values vary as a function of the alkoxysilane precursor and are more sharpened with the increasing of hydrocarbon chain.

It can be noticed that the decomposition peak of physically adsorbed ammonium (around 350 °C in Cl30B) became weaker and occurs more quickly for the modified clays due the silylation reaction, replacing the physically adsorbed ammonium (Qian et al. 2009; Zhang et al. 2006).

Table 2 The mass losses of the reference and silylated samples in the range of 100–900 °C

Cloisite type	Cl30B	Cl30B-Vy	Cl30B-Ph	Cl30B-C8	Cl30B-C18
W = weight loss between 200 and 900 °C (%)	21.94	28.41	29.07	28.59	32.04
$W' = W_{\text{Cl30B-R}} - W_{\text{Cl30B}}$ (%)	0	6.47	7.13	6.65	10.1
R = Vy, Ph, C8, C18					
Silylation degree (moles organosilyl group grafted on 1 mol of Cl30B)	–	0.59	0.41	0.30	0.26

Table 2 summarizes the weight losses of the reference (Cl30B) and that of the silylated samples in the range of 100–900 °C. We assume that the weight loss difference between the reference (1) and the silylated sample (2) equals the amount of grafted silane. We have considered only edge reaction while self-condensation, partial face modification, and loss of ammonium salts may also occur (Voorn et al. 2006). The weight loss of the silylated clays increases with the length of hydrocarbon chain, in agreement with the FTIR analysis. Molar weight of Cl30B was approximated by the following procedure: (1) considering the theoretical structure of the montmorillonite (549.07 g/mol); (2) based on the cation exchange capacity (CEC) (90 meq/100 g), the moles number of cationic modifier was calculated per 1 mol of Cl30B; (3) the theoretical molecular weight of the ammonium salt was calculated (methyl, tallow, bis-2-hydroxyethyl); and (4) based on the CEC, it results that 1 mol of Cl30B consist by equivalence in 549.07 g/mol montmorillonite and 181.26 g/mol (0.4942 Eg methyl, tallow, bis-2-hydroxyethyl) of quaternary ammonium salt and finally the molecular weight of Cl30B was estimated to 730.33 g/mol. To assess the moles of organic chain attached to the clay edges, only the grafted group molecular weight was considered (–Si–R, where R = Vy, Ph, C8, C18).

From stoichiometric point of view, it can be observed that the number of moles functional groups is decreasing with the increasing length of the hydrocarbon chain. Thus, the highest degree of functionalization is achieved with vinyldimethylethoxysilane. Although C18 has the lowest molar amount according to TGA, the process is considerable as it was confirmed by FTIR data. TGA results confirm the successful functionalisation of the organo-modified montmorillonites, the degree of silylation increasing from octadecyl to vinyl (and decreases with the length of hydrocarbon chain).

Table 3 The surface energy and its dispersive and polar components of the organo-modified clays used in this study

Clay type	Surface energy (mN/m)		
	Total	Dispersive component	Polar component
Cloisite 30B	41.84	34.27	7.57
Cloisite 30B-Vy	42.73	36.59	6.46
Cloisite 30B-C8	45.01	39.04	5.97
Cloisite 30B-C18	42.51	39.07	3.44

Further information on the functionalization of the organoclays synthesized in this study was obtained from the free surface energy. Observing the free surface energies listed in Table 3, it is clear that Cloisite samples modified with various organic are more hydrophobic compared to the as received Cloisite 30B. The hydrophobicity increases in the order: Cloisite 30B < Cloisite 30B-Vy < Cloisite 30-C8 ~ Cloisite 30-C18, as the dispersive component of the free surface energy increases.

From this stage, based on FTIR, TGA and surface energy analyses, we can anticipate the hydrophobic character as a vectorial result between the length of the hydrocarbon chain and the amount of silane groups grafted onto clay edges. This character acts on the dispersion ability or self-assembling association of the particles in non-polar media. This assumption was confirmed by DLS analyses of the functionalized clays dispersed in CH_2Cl_2. Size distribution (Fig. 4) shows only one generation of particles for all analyzed samples, Cl30B and silylated Cl30B series. The dimensions of the aggregated layers are in good agreement with the ones obtained by TEM (around 100 nm individual layers and between 600 and 2000 nm for the aggregated layers). To a closer inspection, a very interesting shifting of Cl30B-Vy aggregates toward smaller values can be noticed. There is a gradual return toward greater values as the hydrocarbon chain length of the grafted silane increases. In this context, the aggregates tend to

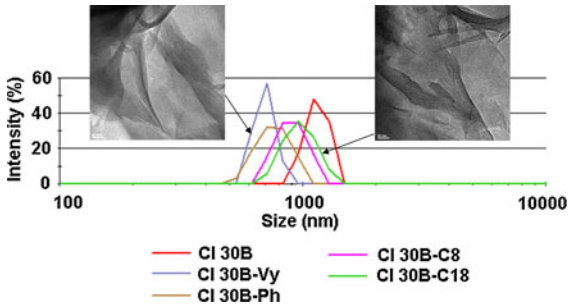

Fig. 4 DLS analyses of Cl30B and silylated Cl30B in dichloromethane with TEM details on the dried Cl30BVy and Cl30BC18 (the *scale bar* is 20 nm)

unpack, because of a high grafting degree of vinyl groups. As the hydrocarbon chain length increase, it is expected for the modified clay particles to posses a higher dispersion capacity in the non-polar CH_2Cl_2. The grafting degree decreases with the length of the chain (see TGA values, Table 2). This is the reason why for the long chain grafted particles, the aggregation tendency is higher than for short chain grafted particles. The particles can associate both on the hydrophobic (hydrocarbon chain) and hydrophilic (clay layers) segments. Unbalancing the equilibrium between these two types of segments turns in a lower stability of the elementary particles, similar to surfactants HLB (Ianchis et al. 2009). The average aggregates diameter drastically decreases from 1,143 nm (Cl30B) to 698 nm Cl30B-Vy (the highest degree of grafting), as well as the polydispersity. For the rest of the samples, the average aggregates diameter increases to 760 nm (Cl30B-Ph), 899 nm (Cl30B-C8), and 977 nm (Cl30B-C18); the peaks are broader, so the polydispersity increases. This is due to the hydrophobic assembling phenomenon of hydrocarbon chains, which is in good agreement with previously reported results (Herrera et al. 2006; Donescu et al. 2011).

Survey and high-resolution photoelectron spectra of C(1s), O(1s), N(1s), and Si(2p) present in the organo-modified clay structure were recorded for the samples Cl30B, Cl30B-Vy, Cl30B-Ph. The XPS data of the silylated clays show modifications of relative concentrations of C, N, O, and Si. A significant increase in relative concentration of silicon at the

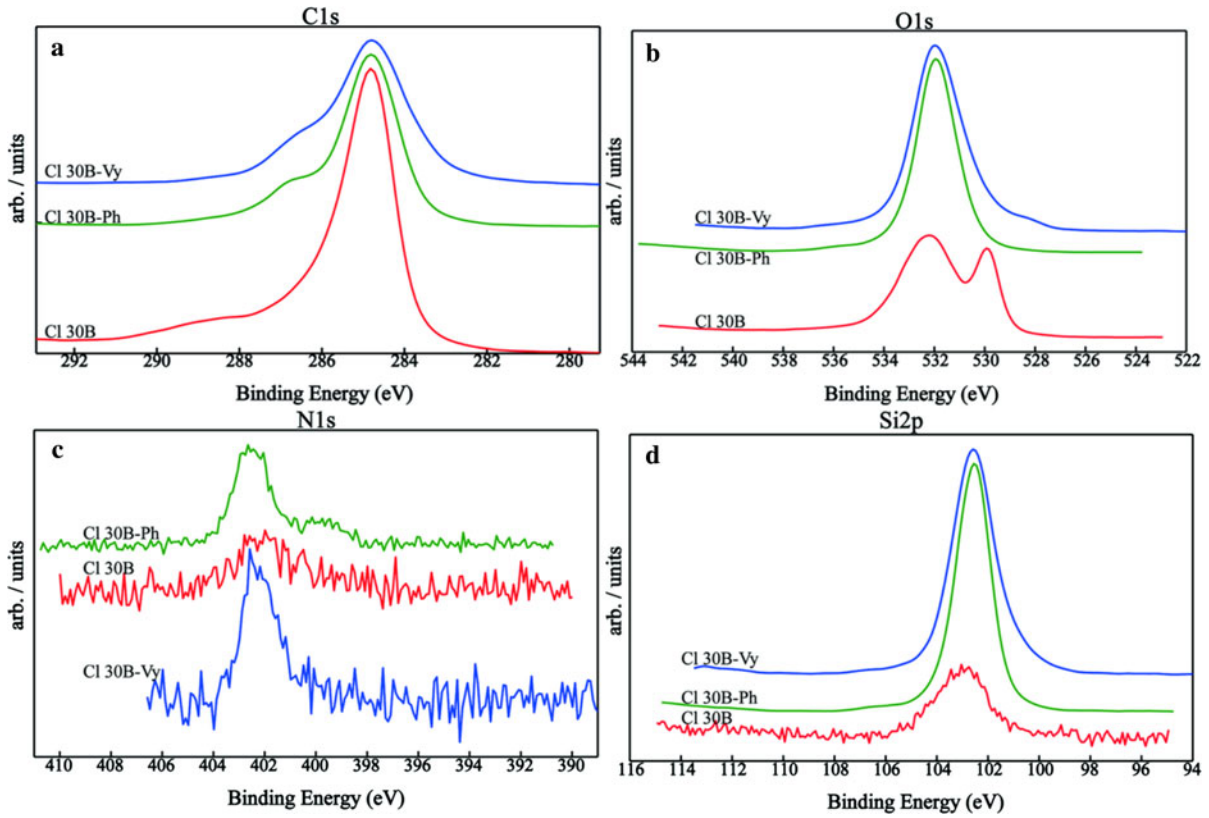

Fig. 5 High-resolution XPS spectra of different samples

surface from 4.36 % (Cloisite 30B) to 12.71 % for Closite 30B-Vy and 13.81 % for Cloisite 30B-Ph was observed. This confirms the silylation reactions. The high-resolution silicon spectrum of Cl30B (Fig. 5d) presents a medium peak at 102.5 eV which can be ascribed to silicates (Rajajeyaganthan et al. 2011; Suzuki et al. 2003; Gusev et al. 2010). The small peak shifting suggests the presence of the silanes (Wilson and Adam 2010). The high-resolution nitrogen spectra of all samples (Fig. 5c) displayed a peak around 402 eV attributed to the organomodifier, respectively, the ammonium salts existing in the clay structure. The change in intensity could be discussed in terms of relative concentration on the surface promoted by layered structure tactoids orientation. The elementary particles (platelets) are associated on the 001 direction (according to the XRD patterns) and are modified with two kind of organomodifiers with different polarities (one the alkyl ammonium salt and second different silanes on the edges). The hydrophobic interaction between these two species (based on the different silane end groups) can promote the alkyl ammonium orientation toward surface.

The high-resolution oxygen spectra of Cl30B (Fig. 5b) presents two peaks: a peak on the left attributed to the OH groups and a second one on the right to the metal oxide (Al_2O_3 for the oxides of iron and magnesium present as isomorphic substitution from clay ionic lattice). After silylation the peak for metal oxide almost vanishes (mainly due to the presence of grafted organic groups, correlated with carbon spectra) and the hydroxyl one shifts toward lower energies as a consequence of Si–O–Si–R formation on the clay surface. This means that can be correlated to the surface signal registered by XPS should be more relevant for the edge of the elementary particles as the surface of the lamella are hindered due the tactoidal association. The initial (Closite 30B) edge groups are hydroxyls from O–Si–OH, O–Al–OH, and O–Mg–OH and this explains the presence of the signal for metal oxides which after grafting and covering with –O–Si-alkyl groups is hindered on the analyzed surface.

The high-resolution carbon spectra of the samples (Fig. 5a) reveal the characteristic peak of carbon at 284.8 eV. The reference sample shows a peak at 289 eV assigned to the C–N, C–O bonding characteristic to ammonium salt structure.

Generally, we observed that the relative concentrations of C and N decrease in favor of O and Si. After

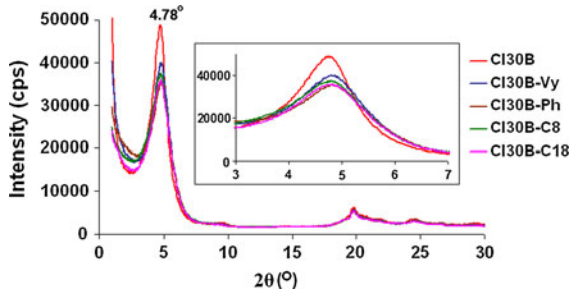

Fig. 6 XRD patterns of Cl30B and silane-modified Cl30B

silylation reaction, it is very possible that the ammonium salts be covered by organosilyl groups, not so rich in C compared to the long alkyl chain ammonium salts and which have the tendency to pack with each other resulting in agglomerated structured as observed by DLS.

From *X-ray* diffraction patterns (Fig. 6), the peaks characteristic to Cl30B are found as follows: a strong peak at 4.78° specific to the basal spacing d_{001} and two small peaks at around 19.8° and 24.5° specific to the 2:1 layer's crystalline structure. As it can be observed, there is almost no change in the d_{001} peak position for all silylated clays. Therefore, there is no increase of the basal spacing in the tactoids after silylation reaction which indicates that the monofunctional alkoxysilanes reacted only by edge covalent bonding and not in between the clay layers, the data being in good agreement with XPS analyses. Judging the decrease in d_{001} peak intensity (meanwhile the other ones are remaining constant), we expect a lower organizing tendency after silylation, or a lower energy in the reforming tactoids. This state suggests further intercalation process with organic molecules. Even if a low amount of ammonium ions could be released in the reaction process, the basal spacing remains unaffected (Zhang et al. 2006; Utracki et al. 2004).

Miniemulsion polymerization

Monomer conversion does not exceed 90 % for styrene polymerization in the presence of Cl30B. By transforming the edges of Cl30B into more hydrophobic structures, the polymerization of styrene can reach higher conversions (El-Sherif and El-Masry 2011; Bourgeat-Lami and Lansalot 2010; Herrera et al. 2006) and consequently offering a better compatibility between clay particles and hydrophobic polymer. For all of our grafted species the monomer conversion was very close to 100 %.

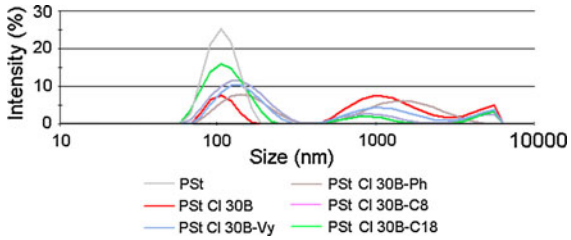

Fig. 7 Size distribution of PSt and PSt composite latexes prepared by miniemulsion polymerization

The latex obtained in the presence of Cl30B and their grafted forms was a white highly homogeneous and dense emulsion. The composite latexes were sized by DLS and their surfaces were analyzed by zeta potential. DLS curves indicate three distinct peaks of particles populations (Fig. 7). There are elementary particles (less than 500 nm), assembled latex particles (between 500 nm and a few microns) and large aggregates area (greater than 3 μm). To depict the influence of the clay modifier, the balance between these three areas and the overall average diameter should be considered. The dimensions of each population are decreasing as the hydrophobic character of the modified clays increases.

The populations of particles presented in Fig. 7 are closely related to the aggregates (second and third peak areas), which are formed by the elementary particles. As the same concentration of latex particles was used for all measurements, one can observe the increase in intensity (with narrower distributions) for the elementary particles (peak area one) as the hydrophobic character of the clay increases. At the same time, the share of the aggregates (peak area two and three) is much decreased. Examining zeta potential profiles (Fig. 8), an important evidence was found regarding the mentioned correlation between elementary particles and aggregates.

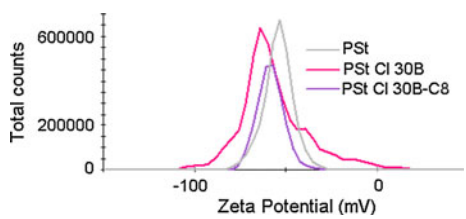

Fig. 8 Zeta potential analyses for PSt, PSt-Cl30B, and PSt-Cl30B-C8 composite latexes prepared by miniemulsion polymerization

The particles surfaces are negatively charged due to the anionic tensioactive agent (SDS) on one hand and to the negatively charged surfaces of the clay particles on the other hand. Zeta potential analysis, also like DLS, can distinguish between populations of particles with different charge levels. In this context, on the Cl30B profile a second weak peak (shoulder) of less charged particle was revealed (Fig. 8). This second peak can be attributed principally to aggregates, where charge compensations are possible, and on the other side to a certain phase (less hydrophobic) of clay layers not so compatible with the polymer particles, which due their polar segments (the surfaces of clay layers) prefer the orientation toward water phase. For all analyzed particles obtained in the presence of edge-modified Cl30B this second peak disappears and the distribution of charges becomes narrower indicating a better compatibility between partners in the nanocomposites latex phase, in good agreement with DLS findings.

The XRD profiles (Fig. 9) indicated that the intercalated polymer phase increases proportionally with the clay hydrophobic modification. In the same time, the expansion of the interbasal spacing d_{001} is much improved for the modified clays compared with Cl30B. This expansion indirectly proves a better compatibility resulted after the advanced organic clay functionalization (from 5.66° to 4.7°). With the modified clays, the amount of intercalated polymer increases in percentage of the ordered phase (see peak intensity) and also in the amount of polymer generated in the interlayer spaces (see peak shift toward greater distances). Moreover, all composites peak widths are

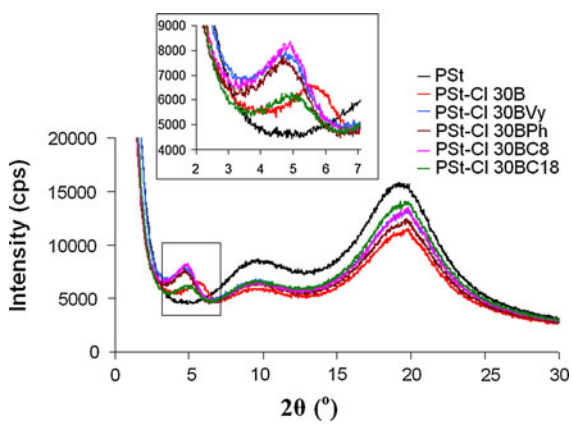

Fig. 9 X-ray diffraction patterns obtained for PSt and PSt composites

increasing in comparison with Cl30B composite, indicating a less organized structure. The overall profiles of the XRD patterns (low intensity peaks for the ordered phase) are suggesting a possible coexistence of exfoliated state for the clay particles showed later in TEM section. However, it is able to offer an increase in basal spacing against Cl30B. Judging only by the hydrophobic level, the observed phenomena seems predictable, but considering also the grafting percentage the swelling ability is lower as compared to

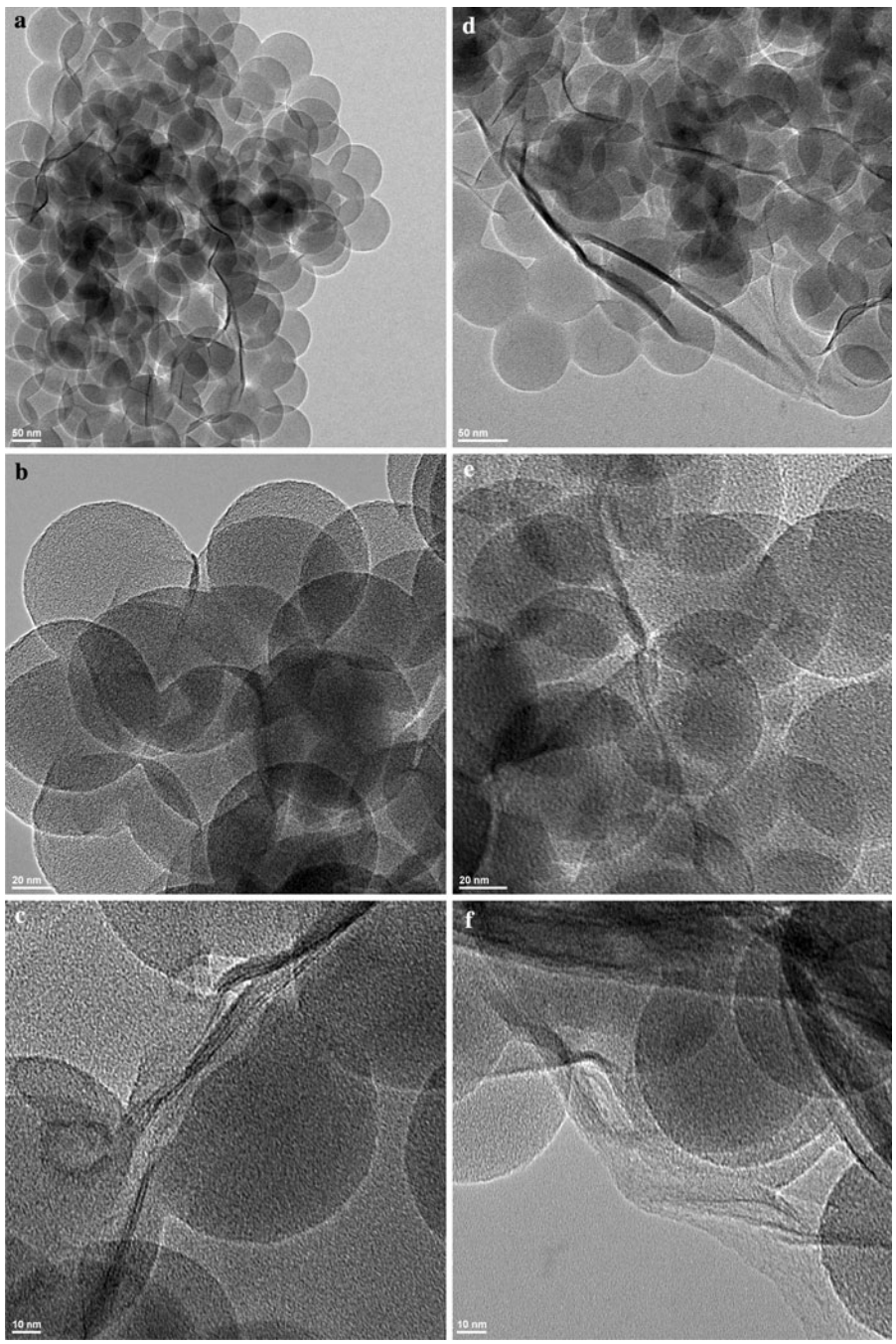

Fig. 10 TEM images for PSt-Cl30BVy (**a–c**) and PSt-Cl30BC18 (**d–f**) nanocomposites

the other modifiers which turns in an overall effect with lower percentage of orientated phase (the intercalated polymer/clay).

TEM images presented in Fig. 10 emphasize the associated morphology induced by all above mentioned interactions. The modified clays appear in intercalated and exfoliated arrangements as well with a good dispersion in the whole nanocomposite phase. HRTEM images revealed the presence of polymer phase onto clay layers separate from the one present as spherical polymer particles (Fig. 10f). The associated morphology in solid state is in good agreement with the dimensional details obtained in latex state by DLS technique. The interlayer expansion of the modified clay, observed in XRD, was also confirmed by TEM pictures.

The presence of clay in the polymer matrix was checked by FTIR analyses (Fig. 11). Cl30B showed the specific peaks of montmorillonite at: 400–600 cm^{-1} (Si–O–Al bending vibration), 1045 cm^{-1} (Si–O stretching vibration), 3635 cm^{-1} (OH stretching of latex water), and around 2930 cm^{-1} (CH_3 stretching vibration from alkyl ammonium salts) (Mirzataheri et al. 2009; Yilmaz et al. 2010). FTIR spectra of polystyrene showed corresponding wavelengths of CH aromatic stretching vibration at 3,020–3,100 cm^{-1}, CH_2 asymmetric stretching vibration 2,850–2,940 cm^{-1}, shearing vibration at 1,450 cm^{-1}, CH aromatic deformation vibration 1,220 cm^{-1}, and vibration of the aromatic nucleus 950–1,050 cm^{-1}. FTIR spectra of polymer–clay nanocomposites reveal the presence of the characteristic peaks of montmorillonite, confirming the inclusion of layered silicates in polymer matrix.

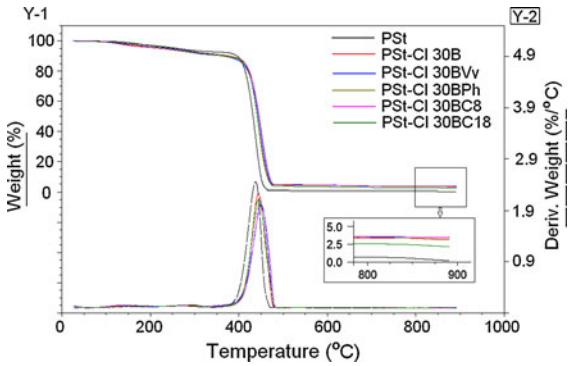

Fig. 12 TGA–DTG curves obtained for PSt and PSt-clay nanocomposites

The presence of montmorillonite in the polymer matrix was supported by TGA analysis, too (Fig. 12). Thermal analysis of the PSt composites samples showed an important growth of final residue from TGA plots. The increased value for the neat polymer from 0.77 wt% up to 3 wt% indicates the presence of the clay (respectively, modified ones) in the polymer matrix.

The presence of clays increases the thermal stability of the polymer, as the T_{max} increases with 10 °C in the presence of Cl30B and up to 16 °C for the silylated samples compared to the plain PSt sample (434 °C). This can be attributed to the presence of organo-modified clay that acts as a diffusion barrier (De Maria et al. 2011). It is worth noting that all silylated samples exhibit greater maximum decomposition temperature than the Cl30B as received. The maximum value was obtained for PSt with Cl30BVy and the minimum for PSt-Cl30BC18. These results correlate well with the

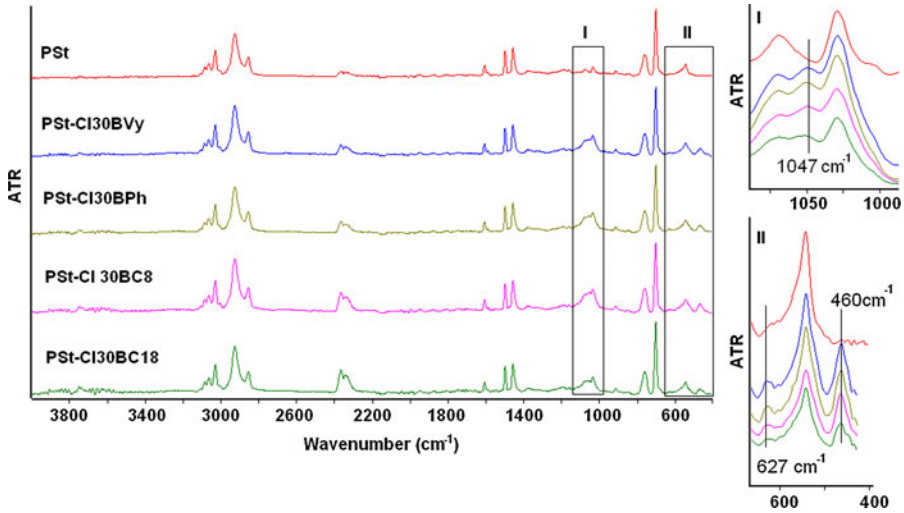

Fig. 11 FTIR spectra of Cl30B, PSt and polymer–clay nanocomposites

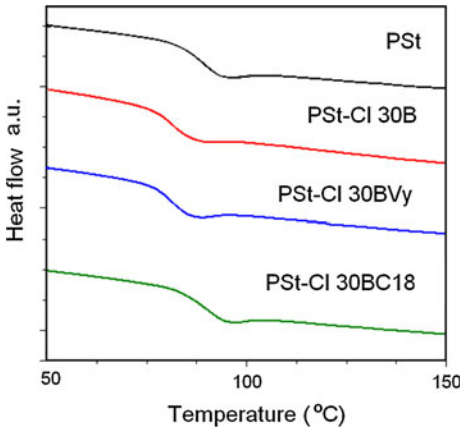

Fig. 13 DSC curves of PSt and some representative PSt-clay nanocomposites

length and grafting degree of the modifiers which in turn affect the interaction/dispersion between partners and thus the morphology of the final nanocomposites.

Glass transition temperature of polystyrene (determined from the second heating ramp, Fig. 13) is also influenced by the presence of clays. Cl30B acts as a plasticizer lowering the T_g of polystyrene from 89 to 81 °C. Adding Cl30BVy, the T_g also decreases at 80 °C as for the Cl30B as received. Interestingly, the T_g of PSt-Cl30BC18 exceeds the PSt-Cl30B value with 8 °C. This phenomenon is due to the presence of C18 long alkyl chain which is very possible to confine the polymer chain.

Conclusions

We have successfully obtained a large variety of functional clay derivatives via silylation reactions of organo-modified clay (Cl30B). The functionalization degree of the clay with several silanes decreased with the increase of hydrocarbon chain length. The assembling process of hydrocarbon chains determines the dispersibility of the clay particles in non-polar media as observed by DLS analyses. Surface energies measurements indicated an increase of the hydrophobic character for the modified clay minerals. FTIR, TGA, and XPS data confirmed the grafting of silane groups onto the clay surface. The monofunctional alkoxysilanes reacted only by edge covalent bonding and not in between the clay layers as confirmed by XRD.

Modified clay/polymer nanocomposites were obtained via miniemulsion polymerization of polystyrene in the presence of several silylated clays. XRD profiles indicated that the intercalated polymer phase increases proportionally with the clay hydrophobic modification. HRTEM images revealed the presence of a distinct polymer phase onto clay layers, beside the polymer phase from the spherical particles. The organomodification improves the thermal stability of polystyrene as showed by TGA.

Acknowledgments The financial support of Executive Agency for Higher Education, Research, Development and Innovation Funding postdoctoral Grants PNII-RU No. 44 (PD_206)/2010 is gratefully acknowledged. The financial support of European Social Fund—"Cristofor I. Simionescu" Postdoctoral Fellowship Programme (ID POSDRU/89/1.5/S/55216), Sectoral Operational Programme Human Resources Development 2007–2013 is acknowledged. M. C. Corobea, announces the partial support of this work by a Grant of the Romanian National Authority for Scientific Research, CNDI-UEFISCDI, Project Number PCCA 137/2012.

References

Bitinis N, Hernandez M, Verdejo R, Kenny JM, Lopez-Manchado MA (2011) Recent advances in clay/polymer nanocomposites. Adv Mater 23:5229–5236

Bourgeat-Lami E, Lansalot M (2010) Organic/inorganic composite latexes: the marriage of emulsion polymerization and inorganic chemistry. In: Van Herk AM, Landfester K (eds) Hybrid latex particles preparation with (mini)emulsion polymerization. Springer, Heidelberg, p 98

De Maria A, Aurora A, Montone A, Tapfer L, Pesce E, Balboni R, Schwarz M, Borriello C (2011) Synthesis and characterization of PMMA/silylated MMTs. J Nanopart Res 13:6049–6058

Donescu D, Somoghi R, Nistor CL, Ianchis R, Ghiurea M, Prodan G, Radovici C (2011) Copolymerization in dispersion of divinyl benzene–maleic anhydride in the presence of silylated montmorillonite clays. Polym Bull 68:993–1007

El-Sherif H, El-Masry M (2011) Superabsorbent nanocomposite hydrogels based on intercalation of chitosan into activated bentonite. Polym Bull 66:721–734

Faucheu J, Gauthier C, Chazeau C, Cavaille L, Mellon J-Y, Bourgeat-Lami E (2010) Miniemulsion polymerization for synthesis of structured clay/polymer nanocomposites: short review and recent advances. Polymer 51:6–17

Gusev EP, Iwai H, Kwong DL, Ozturk MC, Roozeboom F, Timans PJ, Narayanan V (2010) Advanced gate stack, source/drain, and channel engineering for Si. The Electrochemical Society, Pennington, NJ

Herrera NN, Letoffe J-M, Putaux J-L, David L, Bourgeat-Lami E (2004) Aqueous dispersion of silane-functionalized laponite clay platelets. A first step toward the elaboration of water-based polymer/clay nanocomposites. Langmuir 20:1564–1571

Herrera NN, Putaux JL, Bourgeat-Lami E (2006) Synthesis of polymer/laponite nanocomposite latex particles via emulsion polymerization using silylated and cation exchanged laponite clay platelets. Prog Solid State Chem 34:121–137

Hu J, Chen M, Wu L (2010) Organic–inorganic nanocomposites synthesized via miniemulsion polymerization. Polym Chem 2:760–772

Ianchis R, Donescu D, Petcu C, Ghiurea M, Anghel DF, Stanga G, Marcu A (2009) Surfactant-free emulsion polymerization of styrene in the presence of silylated montmorillonite. Appl Clay Sci 45:164–170

Ianchis R, Cinteza LO, Donescu D, Petcu C, Corobea MC, Ghiurea M, Somoghi R, Spataru C (2011) Implications of silylated montmorillonite on montmorillonite polyacrylate-nanocomposites. Appl Clay Sci 52:96–103

Landfester K, Weiss CK (2010) Encapsulation by miniemulsion polymerization. Adv Polym Sci 229:1–49

Lungu AM, Perrin FX, Belec L, Sarbu A, Teodorescu M (2012) Kaolin/poly(acrylic acid) composites as precursors for porous kaolin ceramics. Appl Clay Sci 62–63:63–69

Mirzataheri M, Mahdavian AR, Atai M (2009) Nanocomposite particles with core–shell morphology IV: an efficient approach to the encapsulation of Cloisite 30B by poly(styrene-*co*-butyl acrylate) and preparation of its nanocomposite latex via miniemulsion polymerization. Colloid Polym Sci 287:725–732

Mittal V (2010) Polymer nanocomposites by emulsion and suspension polymerization. RSC Publishing, London

Moraes RP, Santos AM, Olivelra PC, Souza FCT, Do Amoral M, Volera TS (2006) Poly(styrene-*co*-butyl acrylate)-Brazilian montmorillonite nanocomposites, synthesis of hybrid latexes via miniemulsion polymerization. Macromol Symp 245:106–115

Owens DK, Wendt RC (1969) Estimation of the surface free energy of polymers. J Appl Polym Sci 13:1741

Paiva LB, Morales AR, Díaz FRV (2008) Organoclays: properties, preparation and applications. Appl Clay Sci 42:8–24

Piscitelli F, Posocco P, Toth R, Fermeglia M, Pricl S, Mensitieri G, Lavorgna M (2010) Sodium montmorillonite silylation: unexpected effect of the aminosilane chain length. J Colloid Interface Sci 351:108–115

Qian Z, Zhou H, Xu X, Ding Y, Zhang S, Yang M (2009) Effect of the grafted silane on the dispersion and orientation of clay in polyethylene nanocomposites. Polym Compos 30:1234–1242

Rajajeyaganthan R, Kessler F, De Mour Leal PH, Kühn S, Weibel DE (2011) Surface modification of synthetic polymers using UV photochemistry in the presence of reactive vapours. Macromol Symp 299–300:175–182

Schork FJ, Luo YW, Smulders W, Russum JP, Butte A, Fontenot K (2005) Miniemulsion polymerization. Polym Part 175:129–255

Sun QH, Deng YL, Wang ZL (2004) Synthesis and characterization of polystyrene-encapsuylate laponite composites via minimeulsion polymerization. Macromol Mater Eng 289:288–295

Suzuki S, Yanagihara K, Yamazaki S, Tanaka K, Waseda Y (2003) SIMS/XPS characterization of surface layers formed in 3 mass% Si-steel by annealing in oxygen at low partial pressure. Surf Interface Anal 35:276–281

Tong Z, Deng Y (2006) Synthesis of water-based polystyrene-nanoclay composite suspension via mini-emulsion polymerization. Ind Eng Chem Res 45:2641–2645

Utracki LA (2004) Clay containing polymeric nanocomposites. Rapra Technology, Shabury, Shrewbury, Shropshire, UK

Voorn DJ, Ming M, Van Herk AM (2006) Clay platelets encapsulated inside latex particles. Macromolecules 39: 4654–4656

Wan C, Bao X, Zhao F, Kandasubramanian B, Duggan MP (2008) Morphology and properties of silane-modified montmorillonite clays and clay/PBT composites. J Appl Polym Sci 110:550–557

Wilson K, Adam L (2010) Applications of XPS to the study of inorganic compounds. In: Yarwood J, Douthwaite R, Duckett S (eds) Spectroscopic properties of inorganic and organometallic compounds. RSC Publishing, London, pp 72–86

Xu X, Ding J, Qian Z, Wang F, Wen B, Zhou H, Zhang S, Yang M (2009) Degradation of poly(ethylene terephthalate)/clay nanocomposites during melt extrusion: effect of clay catalysis and chain extension. Polym Degrad Stab 94:113–123

Yilmaz O, Cheaburu CN, Duraccio D, Gulumser G, Vasile C (2010) Preparation of stable acrylate/montmorillonite nanocomposite latex via in situ batch emulsion polymerization: effect of clay types. Appl Clay Sci 49:288–297

Zhang J, Gupta KR, Wilkie AC (2006) Controlled silylation of montmorillonite and its polyethylene nanocomposites. Polymer 47:4537–4543